Research Article / Review Article FUPRE JOURNAL 9(1):132-153(2025)

FUPRE Journal

of

Scientific and Industrial Research

ISSN: 2579-1184(Print) ISSN: 2578-1129 (Online)

http://fupre.edu.ng/journal

Sequestration of Methylene Blue from aqueous solution by cellulose of Sand box *(Hura crepitans L.)* seed shells

ALABI-ABASS, M. O.[1,*], *BABARINDE, N. A. A.*[1], *IBIKUNLE, A. A. .*[1]

[1]*Chemical Sciences Department, Olabisi Onabanjo University, Ago-Iwoye, Ogun State.*

ARTICLE INFO

Received: 20/12/2024
Accepted: 02/04/2025

Keywords

Adsorption, Cellulose, Desorption Hura crepitans, methylene blue

ABSTRACT

The capacity of cellulose from sand box (*Hura crepitans*) (HC) seed shells for the removal of Methylene blue dye from aqueous solutions was examined. FTIR and XRD analysis showed functional groups and crystalline nature of the cellulose. Utilising Scanning Electron Microscopy (SEM), the porosity of the adsorbent was examined. Using 0.5 g mass of the adsorbent at pH 12.0, initial dye concentration of 20 mgL^{-1}, contact period of 120 min and temperature of 25 °C, the adsorption parameters showed the greatest dye removal effectiveness of 98.41%. The kinetic models of Pseudo-First order, Pseudo-Second order and Intra-particle diffusion were used. Whereas the Langmuir, Freundlich, Temkin, and Dubinin-Radushkevich isotherms were used to fit the equilibrium data. The kinetic data best suited the Pseudo-Second order model, whereas the Langmuir isotherm most accurately reflected the equilibrium data. Thermodynamic parameters observed are ΔH^o (1.550 $kJmol^{-1}$), ΔS^o (1.846 $Jmol^{-1}K^{-1}$) and $\Delta G°$ (1.013 $kJmol^{-1}$), respectively. Methylene blue adsorption is endothermic and spontaneous, according to these values. 93.05% of the adsorbent was recovered according to the desorption study. Thus, cellulose derived from *Hura crepitans* (HC) is a very effective choice for adsorbents used in the removal of pollutants and dyes in solution.

1. INTRODUCTION

The overwhelming abundance and importance of water, make it indispensable. Water serves as a solvent for major reactions and media, the issue of water pollution has generated major life-threatening challenges globally. Various regulatory bodies in different countries have developed ways of preventing the continuous abuse of wastewater being discharged into the environmental water bodies. These major abuses are being recorded in developing and underdeveloped countries (Wang, 2018). Most industries release effluents that contain hazardous and non-biodegradable chemicals (Fernandes, *et al.* 2021). Highly stable inorganic and organic compounds with inert qualities are released along with heavy metals from the metal processing and dyes from textile and paint industries (Aljeboree *et*

*Corresponding author, e-mail: alabiabassmuibat@gmail.com
DIO

al. 2017). Some other compounds that are found in the water bodies includes agrochemical materials, pesticide residues *suited*, pharmaceutical wastes and domestic waste are generated from their industries or other human activities (Fernández-Ramos *et al.* 2020).

These dyes are often resistant to degradation, resulting in long-lasting contamination that raises chemical oxygen demand (COD), depleting oxygen levels necessary for aquatic life (Gautam, *et al.* 2013; Manzar, *et al*. 2021). Additionally, the presence of dyes can hinder sunlight penetration, affecting photosynthesis in aquatic plants and leading to further ecological imbalances. The foul odours associated with these pollutants can also degrade water quality and affect nearby communities (Prado, 2008). Dyes can have severe hazardous effects on human health, including: damage of the kidney, liver, reproductive system, brain and central nervous system (Midha and Dey, 2009, Oninla *et al.* 2018). Awareness of these risks underscores the importance of proper handling and treatment of dye wastewater to safeguard the environment and human well-being.

Agricultural residues, some of which are cereal husks, sugarcane bagasse, vegetable and fruit peels, legume haulms, roots and tuber peels, palm kernel shells and nuts, often pose significant challenges to environmental sustainability. They often burnt and contribute to accumulation of green-house gases and climate change (Ugwuoke, *et al.* 2018). Some of these wastes are not suitable for making animal feed or economically beneficial (Ibikunle *et al.* 2023).

Treating wastewater containing dyes is indeed a significant challenge, and traditional methods such as coagulation, membrane filtration, aerobic and anaerobic degradation and chemical treatments often fall short in terms of effectiveness, affordability and flexibility (McKew *et al.* 2013; Bazrafshan *et al.* 2015). Although activated carbon is a popular adsorbent for removing dyes, its scalability is limited by its high running costs and regeneration requirement (Iqbal *et al.* 2009). Adsorption is regarded as a dependable and effective technique for treating wastewater contaminants due to its affordability and ease of use (Rangabhashiyam, *et al*. 2022). Different adsorbents such as sugarcane leaf-biomass (Adigun, *et al.* 2020) biogas wastes-slurry, tree-fern (Ho, *et al.* 2005), moss (Low, *et al.* 1995), bacteria (Arami, *et al.* 2005) and coffee wastes (Aksu, and Isoglu, 2007) has been used by researchers. However, more efficient and excellent adsorbents are still being explored.

Hura crepitans, a non-edible plant and commonly known as sandbox tree or possum-wood, belongs to the Euphorbiaceae family that grow in the tropical regions of the world (Fowomola and Akindahunsi, 2007). It produces distinctive pumpkin-shaped seed pods that transits from green to brown. While the oil extracted from its seeds is toxic and can lead to severe health issues, including corneal damage upon contact with the eyes (James, 2013). Despite its toxicity, *Hura crepitans* has potential for industrial applications, particularly in producing adsorbent materials or bioactive compounds but these have not been greatly harnessed (Nsi *et al.* 2018). Therefore, this study is aimed at the useful conversion of *Hura crepitans* into cellulose as an excellent adsorbent to efficiently clean up dyes and contaminants in wastewater.

2. MATERIALS AND METHODS

2.1 Materials

The ripe sand-box seed (*Hura crepitans)* shells, used as adsorbent in this study were collected from its tree base found in the premises of Olabisi Onabanjo University

mini-campus Ago-Iwoye, Ogun State, Nigeria. Methylene blue dye with molecular formula $C_{16}H_{18}ClN_3S$ and mass 319.86 $gmol^{-1}$ of analytical grade is obtained from Sigma Aldrich, United Kingdom. Double-distilled water was utilised for the duration of the investigation, and the other reagents employed are also of analytical grade.

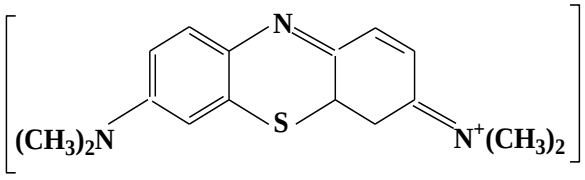

Figure 1. Structure of methylene blue

2.2 Adsorbent Preparation

The *Hura crepitans* (HC) samples were properly cleaned to remove any dirt or sand particles using double-distilled water. It was then sun dried to obtain the actual plant material with lesser moisture content. Sand-box seed shells are hard shells, it was further crushed and pulverized by a locally fabricated grinding and milling machine. These pulverized sample was then sieved with a mesh of very small pore size (10 – 20 μm) to obtain adsorbent particle with larger surface area and smoothness. It was kept in an airtight container for subsequent use.

2.2.1 Cellulose Isolation

Isolation of cellulose was done by using the method of Alabi-Abass *et al.* (2016) adopted from the style of (Alemdar and Sain, 2008b) with modifications. It involves delignification of the cellulosic material by alkaline hydrolysis. The pulverized sample was soaked in double distilled water for 24 h at 25 ℃ to raise the surface of the cellulosic material, increase particle size and separate undesired colour. It was then delignified with 20 % sodium hydroxide for 1h 30 min at 70 ℃ and repeatedly rinsed with double-distilled water until the filtrate had a litmus-neutral consistency. This delignified cellulose was then subjected to bleaching by using 3.5% sodium hypochlorite for 30 min at 30 ℃ to obtain a brightly coloured cellulose adsorbent tagged HC.

2.3 Cellulose Characterization

The Shimadzu FTIR 8400 S Fourier transform Infrared Spectrophotometer was employed. Samples weighing 0.01 g were homogenised using mortar agate and 0.01 g KBr anhydrous. The mixtures were scanned in the 600–4000 cm^{-1} wavenumber range after being compressed by vacuum hydraulic (Graseby Specac) at 1.2 psi to produce a transparent pellet. The sample's porous nature was ascertained by analysing its surface morphology. The analysis was conducted using the Phenom Prox model, Scanning Electron Microscope paired with Energy Dispersive X-ray Spectroscope (SEM-EDS), Eindhoven, Netherlands. The x-ray diffraction (XRD) analysis was used to examine the cellulose sample's crystallinity and amorphous nature. Using the Empyrean Malvern Panalytical X-Ray Diffraction (XRD) System.

2.4 Determination of Point of Zero Charge (pHpzc)

The approach of Banerjee and Chattopadhyaya (2013) was used to estimate the pH at point of zero charge (pHpzc) of HC. 50 mL of a 0.01 M NaCl solution was introduced into 250 mL Erlenmeyer flasks. The initial pH (pHi) of each solution was brought within the range of 2 to 12 by adding either 0.1 M HCl or 0.1 M NaOH solutions. Afterward, each of them received 0.2 g of HC. After 48 h of agitation in each flask, a pH meter (EcoSense pH100A, China) was used to determine the solution's final pH (pH_f). The pHpzc was identified as the curve's point of intersection based on the graph that plotted the pH change against the original pH.

2.5 Preparation of aqueous dye solutions

In order to create the initial stock solutions, 1000 mg of methylene blue (MB) dye were dissolved in 1000 mL of double-distilled water. The stock solutions were diluted to create the experimental solutions, which ranged in concentration from 10 to 100 mgL^{-1}. By adding 0.1 M NaOH or 0.1 M HCl solutions, the pH of the solutions was adjusted and recorded by a pH meter (EcoSense pH100A, China). By applying a UV/Vis Spectrophotometer (UV-1900, British) to quantify the dye solution absorbance, a standard calibration plot was created for methylene blue at λmax, 670 nm.

2.5.1 Batch Adsorption Studies

By examining the impact of crucial variables such as pH, adsorbent dose, contact time, initial dye concentration and temperature on the adsorption process, the ability of HC to remove MB from aqueous solution was examined. Batch adsorption were conducted in 250 mL Erlenmeyer flasks having 50 mL of dyes solution of various pHs (2 - 12), initial dye concentration in the range 10 – 100 mgL^{-1}, adsorbent dose from 0.1 – 1.0 g for 120 min at 25 ℃. The flasks containing the dye solution were thoroughly agitated in an orbital shaking incubator (OS-20Pro, JOANLAB China) at 180 rpm, 25 ℃ for 120 min, respectively. The identical conditions were used for blank solutions, with the exception of adding adsorbent material. 0.1M HCl or NaOH solutions were employed to modify the reaction's pH. The samples were removed after 3 h of agitation and centrifuged for 10 min at 2000 rpm using a centrifuge (TGL-16A, British). The remaining methylene blue dye concentration was then ascertained using the aliquots. Equations (1) and (2) were used to determine the amount of dye adsorbed per unit mass and the percentage of dye removal effectiveness, respectively.

$$\text{Percentage Dye Removal} = \frac{(C_0 - C_e)}{C_0} \times 100 \quad (1)$$

$$q_e = \frac{(C_0 - C_e)V}{W} \quad (2)$$

where the initial and equilibrium dye solution concentrations (mgL^{-1}) are denoted by Co and Ce, respectively.

q_e is the amount/quantity at equilibrium of dye adsorbed on the adsorbent (mgg^{-1}),

v is the volume of dye solution (cm^3)

w is the amount of the adsorbent (g).

2.6 Adsorption Kinetics

Pseudo-fFrst order (PFO) (Simonin, 2016), Pseudo-Second order (PSO) (Parlayici, 2019), and Intra-particle diffusion (IPD) (Campos *et al.* 2018) are the kinetic models applied to the experimental data in order to investigate the rate determining mechanism and the kinetics of MB adsorption onto HC. According to equations (3), (4) and (5), respectively, the linear equations for the Pseudo-First order, Pseudo-Second, and Intra-particle diffusion at equilibrium were computed.

Pseudo-first order:

$$\log(q_e - q_t) = log\, q_e - \frac{k_1}{2.303} t \quad (3)$$

Pseudo-second order:

$$\frac{t}{q_t} = \frac{1}{k_2 q_e^2} + \frac{1}{q_e} t \quad (4)$$

$$\log R = blogt + logk_d \quad (5)$$

Where k_1 and k_2 are PFO and PSO adsorption kinetics constants in (min^{-1} and $g.mg^{-1}$ min respectively, amount adsorbed (mgg–1) with respect to time is denoted by qt and qe, respectively, while Intra-particle diffusion constant (mgg^{-1}min) is denoted by kd.

2.7 Adsorption Isotherm

The maximum adsorption capacity is determined by using the adsorption isotherms, which express the interaction between the adsorbent and adsorbate under steady temperature and equilibrium conditions. Langmuir and Freundlich isotherms were used to calculate the two-parameter adsorption isotherm at the solid-fluid interface (Ng *et al.* 2002), Temkin and Dubinin-Radushkevich (D-R) (Dada *et al*. 2012) by using equations (6 -9).

Langmuir:

$$\frac{1}{q_e} = \frac{1}{q_m} + \frac{1}{q_m K_L} \cdot \frac{1}{C_e} \quad (6)$$

Freundlich:

$$q_e = \log q_e = \frac{1}{n} C_e + \log K_f \quad (7)$$

Temkin:

$$q_e = \beta Ln K_T + \beta Ln C_e \quad (8)$$

Dubinin-Radushkevich (D-R)*:*

$$In q_e = In\, q_m - \beta \varepsilon^2 \quad (9)$$

Where: the monolayer saturation capacity is q_m ($mg.g^{-1}$), K_L is the constant ($L.mg^{-1}$), the concentration at equilibrium is C_e (mgL^{-1}), K_f = Freundlich isotherm constant [($mg.g^{-1}$) ($L/mg^{1/n}$)], n = adsorption intensity indicator, K_T = Temkin isotherm constant, β/R = Universal gas constant (8.314 J mol^{-1} K^{-1}), E = $\frac{1}{\sqrt{2\beta}}$, $\varepsilon = RTIn(1 + \frac{1}{C_e})$, $\beta = constant$ (mol^2/J^2) and E = mean energy ($kJmol^{-1}$).

2.8 Thermodynamics

The process of adsorption is measured by thermodynamic parameters such standard Gibbs free energy (ΔG^o), standard enthalpy (ΔH^o) and standard entropy (ΔS^o). MB adsorption onto HC was studied thermodynamically at temperatures ranging from 298 to 333 K. Equations (10–12) were used to calculate the thermodynamic parameters.

$$K_a = \frac{q_e}{C_e} \quad (10)$$

$$lnK_a = \frac{\Delta S^o}{R} - \frac{\Delta H^o}{RT} \quad (11)$$

$$\Delta G^o = \Delta H^o - T\Delta S^o \quad (12)$$

Where the distribution coefficient is denoted by K_a. The graph of $\frac{1}{T}$ versus lnKa was created using the Van't Hoff equation; the slope's value is ΔH^o and the line's intercept is ΔS^o, respectively.

2.9 Desorption Studies

The reusability efficiency of HC was evaluated by performing desorption study. Desorption of the initially MB adsorbed HC was achieved by using a mixture of 0.1 M HCl and ethanol in ratio 1:1 as the desorption solution. The initially MB adsorbed HC and 50 mL of the mixture, 0.1 M HCl and ethanol mixture was agitated at 180 rpm for 5 h at room temperature. Afterward, the MB adsorbed- desorbed HC was collected and washed severally with double distilled water and further dried at room temperature for the next period of adsorption study. Five cycles of the experiment were conducted and equation (13) was used to determine the desorption efficiency (Ma *et al.* 2022).

Desorption

$$\% = \frac{q_{des}}{q_{ads}} x\ 100 \quad (13)$$

Where q_{des} and q_{ads} represent the quantity (mg/L) of dye desorbed and adsorbed, respectively.

3. RESULTS AND DISCUSSION

3.1 Cellulose Characterization

The FTIR spectra of the MB-loaded (HCS) and unloaded HC are displayed in Figure 2. The spectra display typical spectra at 3792 cm^{-1} caused by O-H stretch of the alcohol group and broad bands at 3233 cm^{-1} attributed to the O-H stretch in carboxylic acid. The carbonyl functional group (C=O) has a characteristic peak at 1633 cm^{-1}, the alkane groups in cellulose have a C-H deformation peak at 1373 cm^{-1} and the alcoholic groups in cellulose have a conspicuous peak at 1057 cm^{-1} that is caused by C-O vibration (Afroze, 2016, Le *et al.* 2021). The N=C=O stretching in the MB-loaded HCS is responsible for the new band observed at 2134 cm^{-1} where changes in peak intensities indicates a physical adsorption process and active interaction of the adsorbent in MB uptake (Degermenci *et al.* 2019). The desorbed spectra also showed representative peaks in cellulose but with increased intensities thus, indicating no deformation of HC and its reusability.

X-ray diffractometry analysis (XRD) was used to investigate the crystallinity and amorphous state of unloaded HC, MB-loaded HCS and MB-desorbed HCD. The diffractograms for unloaded HC, MB-loaded HCS, and MB-desorbed HCD are shown in Figure 3 (a–c), respectively. At 2 Theta = 23°, a noticeable and strong peak indicates the presence of organised crystalline cellulose (Adigun *et al.* 2019). Highly carbonaceous crystalline entities are also depicted by another noticeable, but less significant peak at 2 Theta = 21°. There are several less ordered amorphous molecules, including lignin and polysaccharides, present in the sample, as evidenced by further faint peaks at 2 Theta = 15° and 19° (Reddy *et al.,* 2010; Adigun *et al.*,2019). The crystalline structures in HC and HCS are similar except with the emergence of new angle at 33° with higher intensity in HCS indicating the presence of MB. This suggests that HC is crystalline and was efficient in the uptake of the MB dye in solution. However, this intensity decreased in HCD showing that the MB had been released from its surface (Adigun *et al.* 2020).

Figure 4 (a-c) shows the porous nature and shape of HC before, after adsorption of MB (HCS) and after desorption. Scanning electron microscopy (SEM) technique was used to determine the surface structure and characterize the morphology of the adsorbent. The porosity of the adsorbent enhances the amount of dye that sorbs onto its surface (Hassan and Hossein, 2018) Bulut *et al.* 2011). The surface of the unbounded HC presents large pores of long clustered adsorbent while the dye bound image shows the attachment of granules and the adsorbent now shows a loosen and pore occupied form. These images confirm that the adsorbent had taken up dye by adsorption, similar morphological characteristics exists in other studies (Kebede *et al.* 2018; Hernandes *et al*. 2019). The morphology of MB-desorbed (c) presents HC with more cavities and porous surface (Oninla *et al.* 2018). The appearance of porous cavities in the SEM image of MB-desorbed HCD confirmed the removal of MB from the adsorbent's surface (Adaramola *et al.* 2024). Adsorption is a physical phenomenon that occurs on the surface of an adsorbent. The changes in morphology noticed on the surface of HC before and after adsorption shows the important role that porosity of adsorbent plays in the sorption of dye (Jegede *et al.* 2021).

3.2 Impact of Point of Zero Charge (pHzc) and other parameters on Adsorption

3.2.1 Impact of Point of Zero Charge (pHzc) and pH on Adsorption

The point at which the electrical charge on an adsorbent surface becomes neutral is known as the pHpzc. Electrostatic interaction with cationic methylene blue molecules is promoted when the adsorbent surface is negatively charged (Alshekhli *et al*. 2020). However, the adsorbent surface charge turns positive at pH < pHpzc, it causes the cationic molecules of MB to strongly repel the surface of the adsorbent. The pHpzc of HC was found to be 7.0, as seen in Figure 5a. This suggests

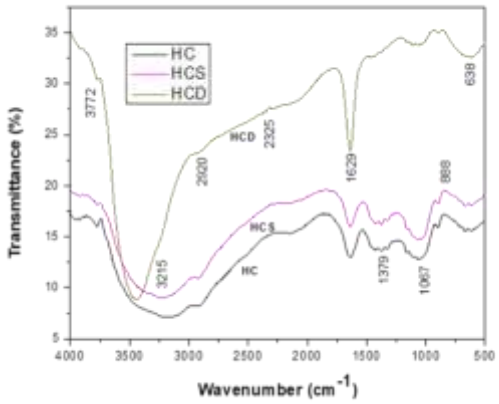

Figure 2. FTIR of (a) unloaded HC (b)MB-loaded HCS and (c) MB-desorbed HCD at pH 12, adsorbent dosage 0.5 g, 25 ℃, 120 min and initial dye concentration 20 mgL^{-1}).

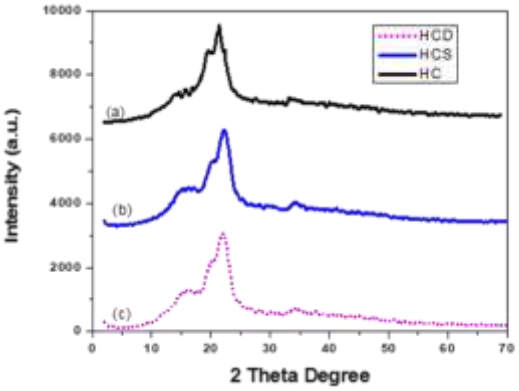

Figure 3. XRD pattern of HC (before MB adsorption), HCS (after MB adsorption) and HCD (after MB- desorption).

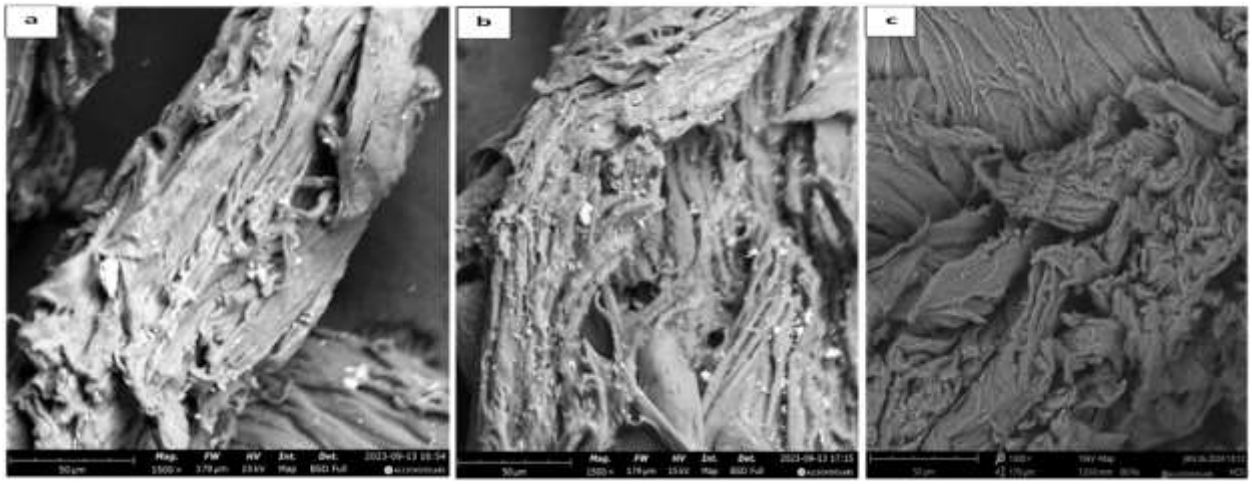

Figure 4. SEM image of (a) unloaded HC, (b) MB-loaded HC and (c) MB-desorbed HC.

that the adsorbent has less acidic sites, which may be related to the presence of some negatively charged functional groups on it. Similar findings have been documented in previous studies. (Degermenci *et al.* 2019; Jawad *et al.* 2020).

The adsorption site undergoes protonation and deprotonation at lower and higher solution pH values, making the pH of the dye solution a crucial factor in dye adsorption onto an adsorbent (Chen *et al*. 2016). The pH of 12.0 was the most favourable for the adsorption of methylene blue by HC, as shown in Figure 5b, similar tendency has been documented (Mustapha *et al.* 2023). The sorption of methylene blue onto HC was found to have a removal efficacy of 75–87% at lower pH values between 2.0 and 9.0. This is due to the cationic dye ions competing with the excess H^+ ions for adsorption sites in an acidic environment. The effectiveness of MB removal was comparatively low at pH < 7.0 but demonstrated a noticeable rise at pH > 7.0 since the pHpzc of HC 7.0. The removal efficiency increased from 89 to 97 % as the pH moved from 10.0 to 12.0 due to the negative charge sites on HC surface, which encourages electrostatic attraction between the negatively charged species and the cationic MB. This increased adsorption peaked at pH 12.0 (Babarinde *et al.* 2013). Previous studies on the adsorption of cationic dyes have documented this pattern (Oladipo and Ifebajo, 2018; Jawada and Abdulhameed, 2020; Yudhanto *et al.* 2023).

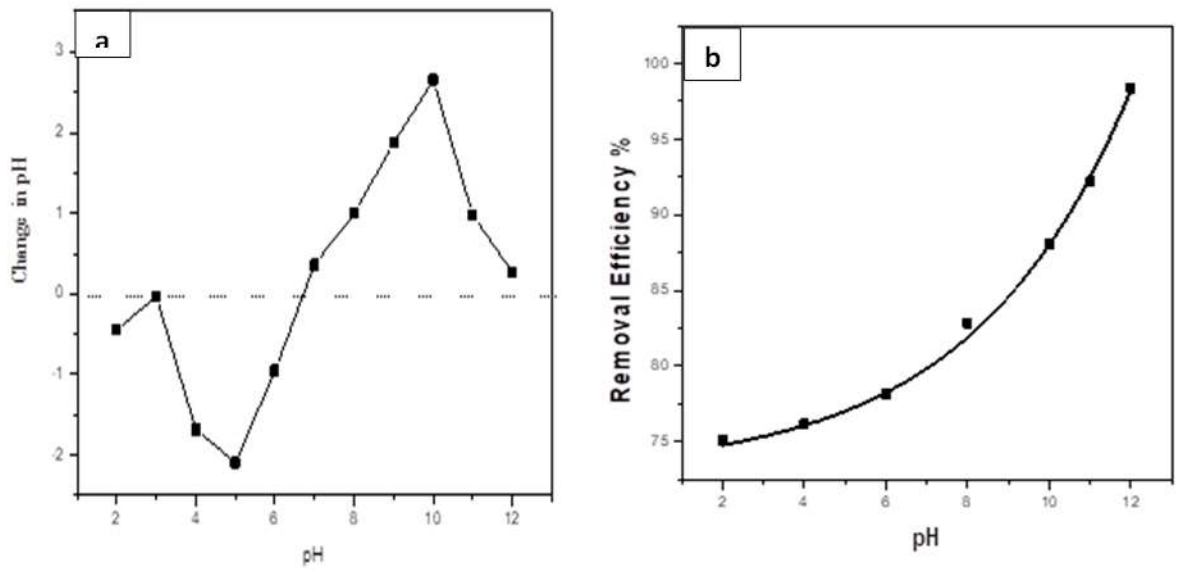

Figure 5. (a) Point of Zero Charge of HC and (b) Effect of pH on HC adsorption of MB (adsorbent dosage 0.5 g, initial MB conc. 20 mgL^{-1} at 25 ^oC).

3.2.2 Impact of Adsorbent Dosage on Adsorption

The impact of adsorbent dose is a key factor influencing the adsorption process. Keeping all other factors same, different amounts of HC (0.1–1.0 g) were examined. Figure 6 depicts that the amount of dye removal increased with the adsorbent dosage, reaching its maximum (98.4%) at 0.5 g. This finding demonstrated that an increase in adsorption capacity emanates from presence of more active binding sites at higher adsorbent doses (Le *et al.* 2012; Nsi *et al.* 2016). However, agglomeration and a decrease in intercellular distance happened at larger adsorbent dosages (0.6–1.0 g),

protecting MB molecules from the HC active binding sites. Consequently, the adsorption efficiency would decline (El-Sikaily *et al.,* 2011).

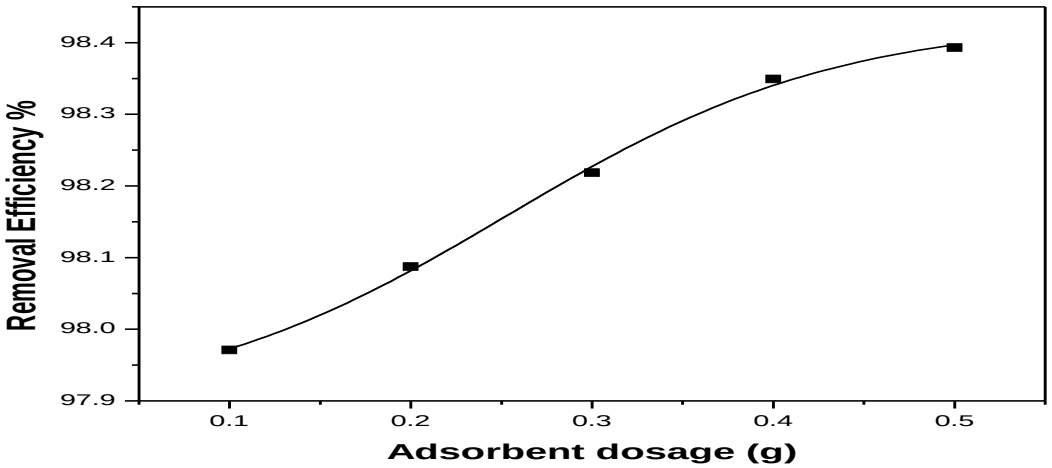

Figure 6. Effect of HC adsorbent dosage (initial MB conc. at 20 mgL^{-1}, pH 12.0 at 25 ºC).

3.2.3 Impact of Contact Time on Adsorption

The amount of MB in percentage removed from the solution is displayed in Figure 7. Initial MB concentrations ranging from 10 to 100 mgL-1 were varied while other adsorption reaction parameters were kept constant. Upon increasing the starting concentration of MB from 20 to 60 mgL^{-1}, the percentage removal decreased from 93.74% for 20 mgL^{-1} to 88.08% for 60 mgL^{-1}, respectively. At higher concentration of MB solution, the removal efficiency was almost at equilibrium and declining due to the increased availability of more dyes on the adsorbent (Zhang *et al.* 2014). A lower pushing force towards the adsorbent's active sites could be the result of more MB molecules being available. Previous studies have been documented (Jawad *et al.* 2020; Paredes-Quevedo *et al.* 2021). According to the data, for all initial dye concentrations with respect to time, a fast adsorption of MB was evident in the first 60 min, which was accompanied by a significantly slower adsorption rate as the time progressed to 120 min. The percentage of dye removal was found to remain constant after 120 min, indicating that this is the ideal equilibrium adsorption time (Azouaou *et al.* 2010). This suggests that there was no apparent dye uptake after the sorption equilibrium time since the biosorbent binding sites significantly decreased (Viswanthan *et al.* 2020).

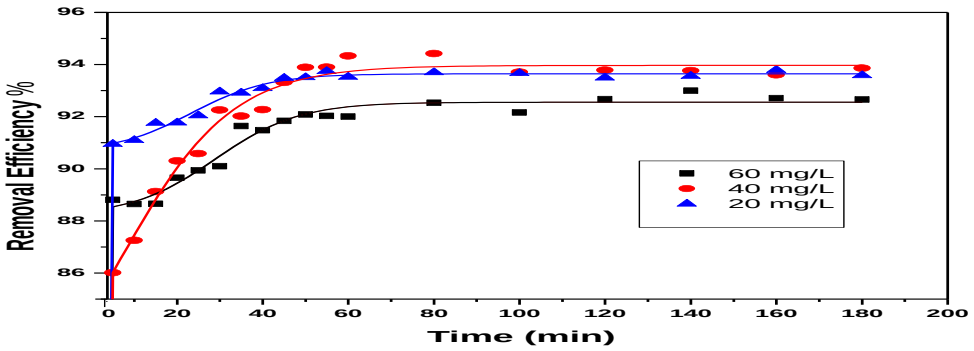

Figure 7. Effect of initial MB concentration and contact time on HC (adsorbent dosage 0.5 g, pH 12.0 and 25 ºC).

3.2.4 Impact of Temperature on Adsorption

The role of temperature in the adsorption process is depicted in Figure 8. The temperature was adjusted between 25 and 60 °C with a starting dye concentration of 20 mgL^{-1}, adsorbent dose of 0.5 g, pH set at 12.0 and contact time of 120 min. The outcome shows that the adsorption capacity increased from 93.0 to 93.4 % as the temperature increased. This suggested that MB's adsorption onto HC is an endothermic process that benefits from increasing temperatures (Banaei *et al.,* 2017).

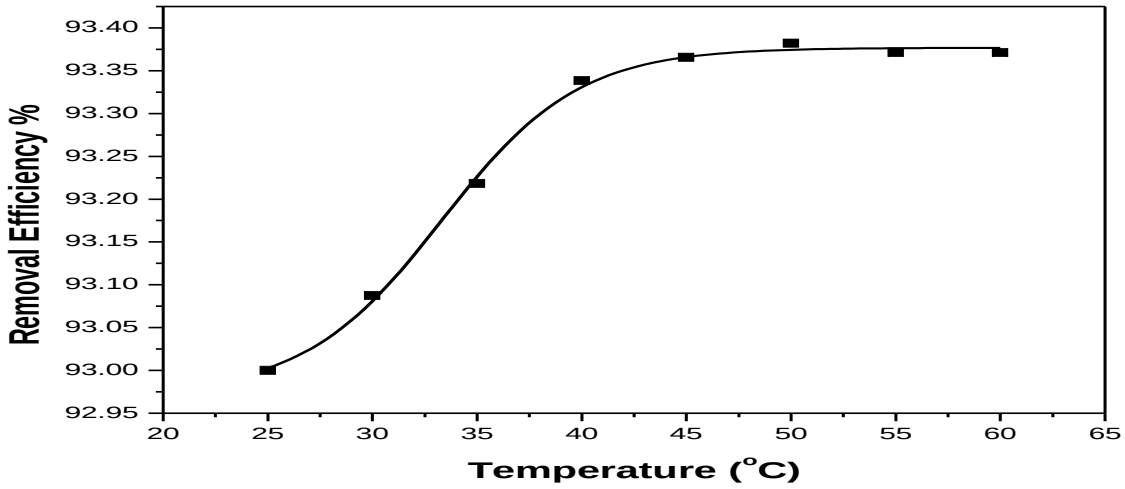

Figure 8. Effect of Temperature on HC (adsorbent dosage 0.5 g, pH 12.0, 120 min, initial MB conc. 20 mgL^{-1}).

3.3 Kinetic Studies

Figures 9 (a–c) display the linear plots of the PFO, PSO and IPD kinetic models and Table 1 lists the kinetic study parameters. The sorption of the solid phase from a liquid phase is the basis of the Pseudo-First order model. The result obtained from this study showed that PFO did not fit the data properly with correlation coefficient (R^2) value being low for the varied concentrations. This was also corroborated with the uptake capacity q_e

*Corresponding author, e-mail: alabiabassmuibat@gmail.com
DIO

experimental and q_e calculated showing significant differences at the various concentrations studied. This clarifies that PFO model is unable to adequately fit the kinetic adsorption data (Tran *et al.* 2017). For all initial MB dye concentrations, the PSO correlation coefficient (R^2) was strong and nearly equal to unity (≥ 0.999) and the predicted adsorption capacities (q_e calculated) and the empirically obtained ones (q_e experimental) corresponded closely. The PSO model is more feasible and favourable than the PFO model for explaining MB adsorption onto the HC. This conforms with other reports (Jawad *et al.* 2018; Ghosh *et al.* 2019; Paredes-Quevedo *et al.* 2021; Mustapha *et al.* 2023). The impact of solute migration from the surface of the adsorbent to the intra-particle active sites through sorption is explained by the Intra-particle diffusion (IPD) kinetic model. Several different diffusion mechanisms are thought to be involved in the variation in the mass transfer rate between the first and last stages of adsorption (Nagy *et al.,* 2014). The quantity adsorbed, qt (mgg^{-1}), plotted against the square root of time has intercepts that do not start at the origin, as seen in Figure 9c. Coefficients of correlation (R^2) were also less than 0.999. Nonetheless, the intercept C value was more than zero, suggesting that the adsorption mechanism involves both intra-particle and external film diffusion (Rangabhashiyam *et al.,* 2022; de Lima *et al*. 2023).

Table 1. The kinetic models and parameters of the adsorption of MB at different initial concentrations.

Kinetic Model	Parameter	C_o		
		20 mgL^{-1}	40 mgL^{-1}	60 mgL^{-1}
Pseudo-first order	$q_{e.exp}$ (mgg^{-1})	0.93786	1.85957	2.76469
	k_1 (min^{-1})	-0.000163	-0.000210	-0.000182
	$q_{e.cal}$ (mgg^{-1})	0.028345	0.164812	0.227556
	R^2	0.649	0.933	0.905
Pseudo-second order	$q_{e.cal}$ ($mgg^{-1)}$	0.939	1.866	2.771
	k_2 (gmg^{-1} min^{-1})	4.049	0.845	0.549
	R^2	0.999	0.999	0.999
Intra-particle diffusion	k_p ($mgg^{-1}min^{-1/2}$)	0.00229	0.0104	0.0105
	C	0.911	1.748	2.641
	R^2	0.699	0.718	0.924

3.4 Isotherm models

The adsorption isotherms explain the link between the maximal adsorption capacity at equilibrium and the adsorbent and adsorbate at constant temperature circumstances. Figure 10 (a-d) illustrates how the Langmuir, Freundlich, Temkin, and Dubinin-Radushkevich isotherms were used to fit the data in this investigation and Table 2 displays the isotherm parameters. Adsorption on homogenous single-layer surface is explained by the Langmuir model. It is not a favourable process if the adsorption process's RL is larger than one (RL > 1), linear if it is equal to one (RL = 1), spontaneous and favourable when RL is between 0 and 1, and irreversible when RL equals zero (RL = 0) (Ooi et al. 2017)

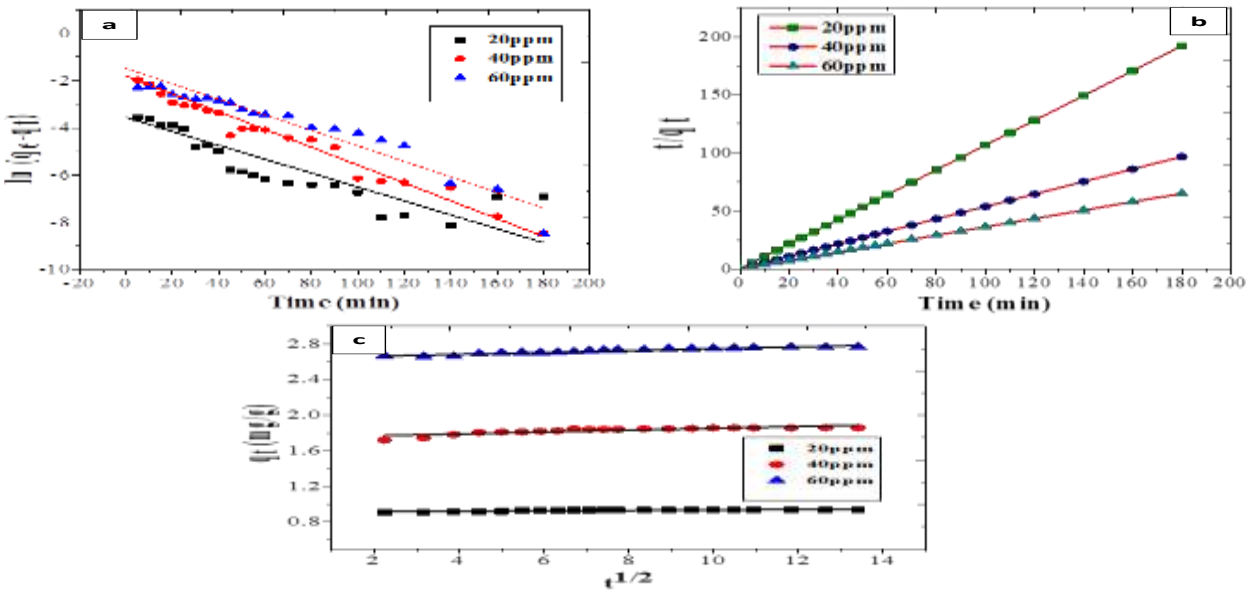

Figure. 9: Linear plots of (a) Pseudo-first order (b) Pseudo-second order and (c) Intra-particle diffusion models of HC at different initial concentrations of MB.

For the constants generated for each parameter with the different isotherm presented in Table 2, the regression line value R^2 (0.9994, 0.993, 0.9639 and 0.8072) obtained for the Langmuir, Freundlich, Temkin and Dubinin-Radushkevich isotherms, respectively. These values present the adsorption as a favourable and spontaneous process for Langmuir, Freundlich and Temkin as they all tend towards 1 except Dubinin-Radushkevich isotherm. However, the Langmuir model predicts more monolayer adsorption because it fits the data the best out of all of them. It also gave an R_L value (0.4231) showing a spontaneous reaction with a capacity removal, q_{max} (12.005 mgg^{-1}). This provides an information that adsorption of MB occurred at the homogenous surface of HC (Azouaou *et al.,* 2010). Comparable reports have been documented (Georgin *et al*., 2019; Le *et al.,* 2021). The heterogeneous adsorption mechanisms and fitting is also described by the Freundlich isotherm showing an *n* value (1.214) greater than 1. Thus, presenting the adsorption of MB onto HC as a physical and favourable (Liu *et al.,* 2018). The Temkin isotherm model demonstrated that MB adsorption onto the HC surface is endothermic and temperature dependant, with a k_T value (1.1594) greater than 1. Dubinin-Radushkevich isotherm presents an E value (1331.56 $kJmol^{-1}$) indicating that MB adsorption onto HC is a chemisorption process (Ooi *et al.,* 2017). In summary, the models that most accurately depict the adsorption mechanism of MB onto HC via the homogeneous and heterogenous surfaces are the Langmuir and Freundlich isotherms.

The adsorption capabilities of various adsorbents for the sequestering methylene blue, as described in the literature, are shown in Table 3. The data obtained for *Hura crepitans* seed shells shows that its capacity compares favourably with some other adsorbents in removing methylene blue from aqueous solutions. It is worthy to note that, *Hura crepitans* seed shells are readily available and eco-friendly alternative adsorbent that poses no risk to human health and the environment.

*Corresponding author, e-mail: alabiabassmuibat@gmail.com
DIO

Table 2. Isotherm models parameters

S/N	Biosorption isotherm	Parameters	Value
1.	Langmuir	q_{max} (mgg^{-1})	12.005
		k_L ($mg.g^{-1}$)	0.0682
		R_L	0.4231
		R^2	0.9994
2.	Freundlich	$\frac{1}{n}$.	0.823
		k_F ($mg.g^{-1}$) (Lmg^{-1})$^{\frac{1}{n}}$	0.783
		n	1.214
		R^2	0.993
3.	Temkin	B_T ($J.mol^{-1}$)	1.801
		K_T ($L.mg^{-1}$)	1.1594
		R^2	0.9639
4	Dubinin–Radushkevich (D–R)	B	2.820×10^{-7}
		q_{max} ($mg.g^{-1}$)	3.112
		E ($kJ.mol^{-1}$)	1331.558
		R^2	0.8072

Table 3. Comparison of various adsorbents' maximal adsorption capabilities for the removal of methylene blue

Adsorbents	**q_{max} (mgg^{-1})**	**Reference**
Bagasse Fly Ash	15.5	Meskel *et al.,* 2023
Iron-oxide nanoparticles	0.230	Yakar et al. 2020
Date stone activated carbon	12.02	Alqaragully, 2014
Raw clay	19.45	Kalipci *et al.,* 2016
Mauritia flexuosa petioles	7.49	Patriota *et al.,* 2020
Sugarcane wastes	17.43	Meili *et al.,* 2019
Bush cane bark	23.49	Enenebeaku *et al.,* 2017
Hura crepitans seed shells	12.05	This study

*Corresponding author, e-mail: alabiabassmuibat@gmail.com
DIO

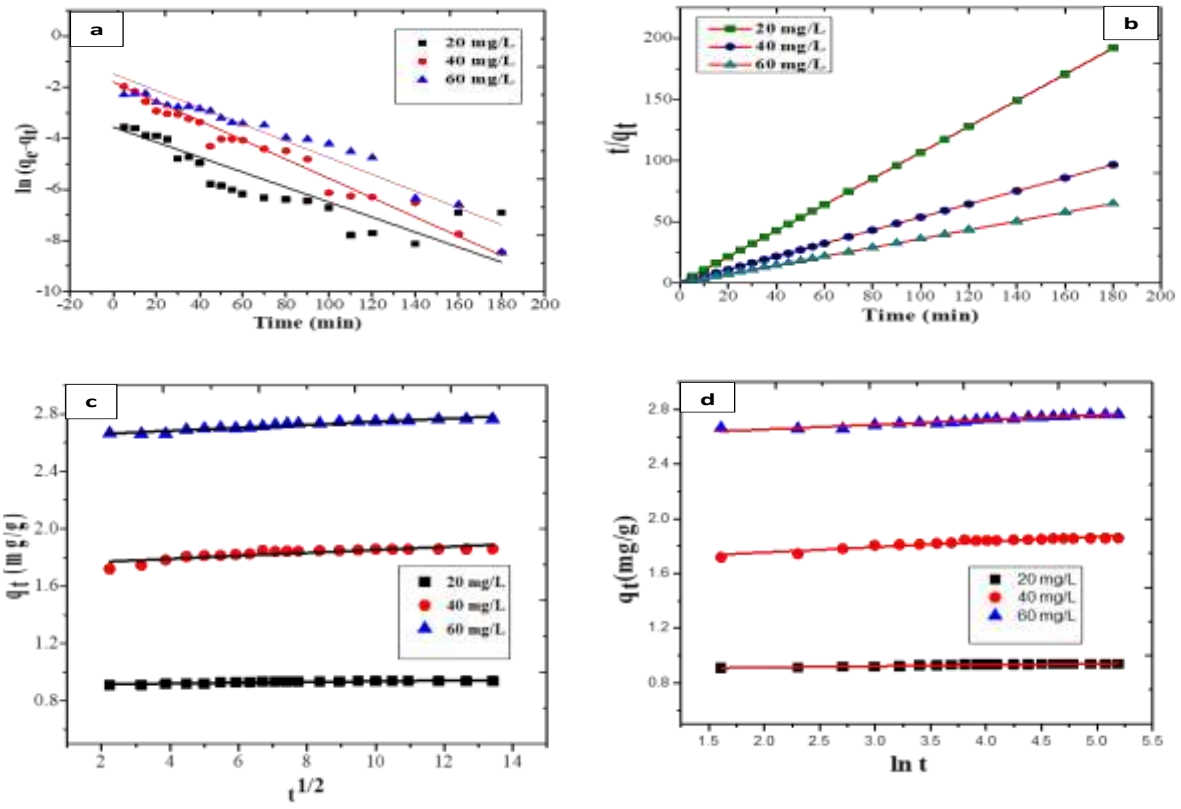

Figure 10. Isotherm model plots of (a) Langmuir (b) Freundlich (c) Temkin and (d) Dubinin-Radushkevich for the adsorption of MB onto HC.

3.5 Thermodynamic Studies

Standard Gibb's free energy change (ΔG°), standard enthalpy change (ΔH°), and standard entropy change (ΔS°) are thermodynamic metrics that provide a clear understanding of the feasibility and spontaneity of an adsorption process. The Vant Hoff's equation graph provided linear plots for the initial MB concentrations taken into consideration. Figure 11 depicts the linear plots while Table 4 gives the thermodynamics parameters. From the results presented, th e positive enthalpy (ΔH°) of the adsorption (+1.550 and +8.837 $kJ.mol^{-1}$) for different initial concentrations of MB indicate the endothermic nature of the process. The adsorption entropy (ΔS°) also has positive values (1.846 and 22.240 $J.mol^{-1}K^{-1}$) reflecting the increase in randomness during the process. Thus, increase in temperature suggests a more favourable condition for driving the adsorption process (Ogundipe and Babarinde, 2017; Oninla *et al.,* 2018; Adigun *et al.,* 2020). The values of ΔG^o in this investigation spans from 0.926 to 2.139 $kJ.mol^{-1}$. These findings are consistent with the MB's spontaneous physiosorption, when ΔG^o falls in the range (2.1–20.9$kJmol^{-1}$) (Mahmoud and El-Halwany 2014; Rudi *et al.* 2020). At elevated temperatures, more effective adsorption is indicated by the decrease in ΔG^o with increasing temperature (Sims *et al.,* 2019).

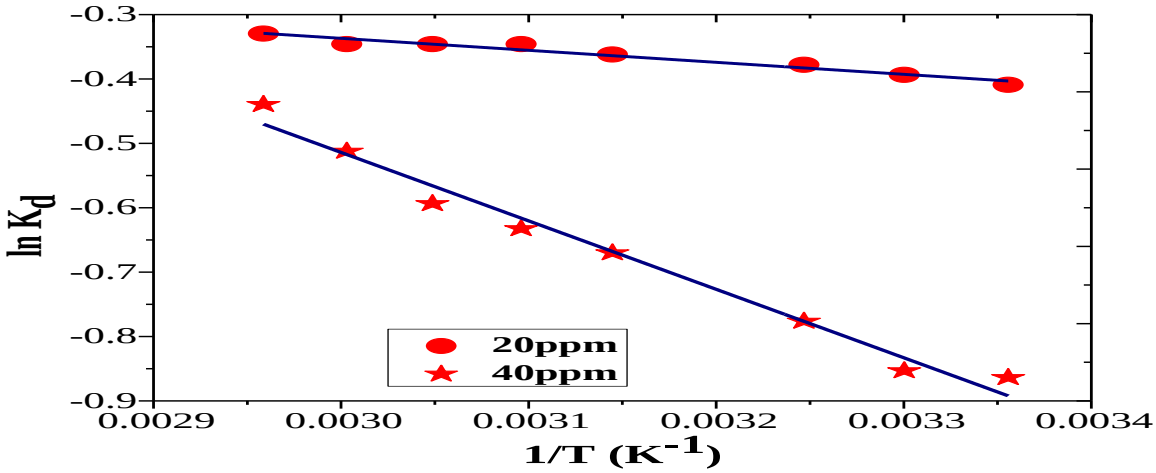

Figure 11. The Van't Hoff's plot for the adsorption of MB onto HC at different initial concentrations.

Table 4. Thermodynamics parameters of the adsorption of MB onto HC at varied temperatures and different initial concentrations.

MB Conc (mg/L)	Parameters								
	ΔH° (kJ.mol^{-1})	ΔS° (Jmol^{-1}K^{-1})	ΔG° (kJ.mol^{-1})						
			298 K	303 K	308 K	318 K	323 K	328 K	333 K	338 K
20	+1.550	1.846	1.013	0.991	0.968	0.957	0.929	0.943	0.958	0.926
40	+8.837	22.240	2.139	2.148	1.987	1.771	1.698	1.618	1.417	1.235

3.6 Desorption and Reusability Studies

Figure 12 displays the outcome of the desorption and reusability procedure for the number of cycles versus the percentage desorbed (removed). Following five consecutive cycles of the adsorption-desorption procedure by adding 0.1 M HCl: ethanol solution, the desorption of MB was greater than 90%. In the subsequent desorption cycles, it decreased to 89.4 and 88.5 % for the fourth and fifth cycles respectively. This finding suggests that MB removal by regenerated HC may be a recurring and effective adsorbent for a continuous process. These results are consistent with those documented in other studies (Pavan *et al.* 2008; Somsesta *et al.* 2020; Ma *et al.* 2022).

*Corresponding author, e-mail: alabiabassmuibat@gmail.com
DIO

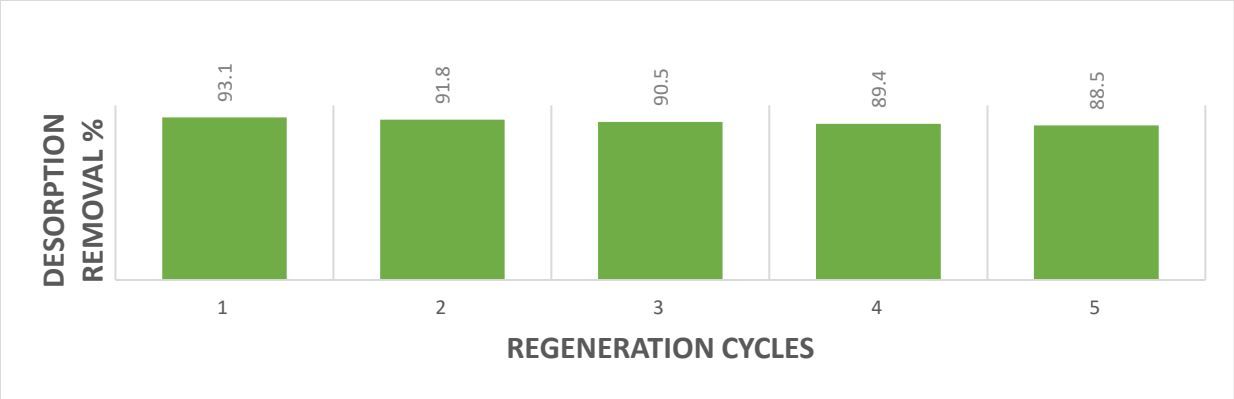

Figure 12. Regeneration study of MB-loaded HC carried out in five adsorption-desorption cycles with 0.1 M HCl-ethanol solution at 25℃ for 5 h.

4. CONCLUSION

The widely available and underutilised cellulose obtained by alkaline hydrolysis of *Hura crepitans* seed shells was effectively employed as an adsorbing material for methylene blue. Batch adsorption method was adopted and carried out at optimum conditions of pH 12.0, adsorbent dosage of 0.5 g, initial MB concentration of 20 mgL^{-1}, contact time of 120 min and temperature of 25 ℃. The FTIR spectra demonstrated the adsorption of the adsorbent by changes in the intensities of specific functional groups. The binding of MB onto the surface of HC is further confirmed by a change in the appearance of the SEM images obtained prior to and after adsorption. The Pseudo-second order model was the most suitable mechanism for the adsorption kinetics, whereas the Langmuir model best fit the data from the adsorption equilibrium. Methylene blue dye adsorption onto HC adsorbent was shown to be feasible, spontaneous, and endothermic based on the results of the thermodynamics investigations. *Hura crepitans* seed shells were therefore discovered to be successful in removing methylene blue from aqueous solution, and they might be used to create a system that effectively removes dyes from contaminated water in the environment.

REFERENCES

Adigun, O. A., Oninla, V. O., and Babarinde, N. A. (2019). Application of sugarcane leaves as biomass in the removal of cadmium (II), lead (II) and zinc (II) ions from polluted water. *International Journal of Energy and Water Resources*, *3*, 141-152.

Adigun, O. A., Oninla, V. O., Babarinde, N. A., Oyedotun, K. O., and Manyala, N. (2020). Characterization of sugarcane leaf-biomass and investigation of its efficiency in removing Nickel (II), Chromium (III) and Cobalt (II) ions from polluted water. *Surfaces and Interfaces*, *20*, 100621.

Afroze, S., Sen, T. K., Ang, M., and Nishioka, H. (2016). Adsorption of methylene blue dye from aqueous solution by novel biomass Eucalyptus sheathiana bark: equilibrium, kinetics, thermodynamics and mechanism. *Desalination and water treatment*, *57*(13), 5858-5878.

Agarwal, U. P., McSweeny, J. D., and Ralph, S. A. (2011). FT–Raman investigation of milled-wood lignins: softwood, hardwood, and chemically modified black spruce

lignins. *Journal of Wood Chemistry and Technology*, *31*(4), 324-344.

Al-Degs, Y., Khraisheh, M. A. M., Allen, S. J., and Ahmad, M. N. A. (2001). Sorption behavior of cationic and anionic dyes from aqueous solution on different types of activated carbons. *Separation Science and Technology*, *36*(1), 91-102.

Aksu, Z., and Isoglu, I. A. (2007). Use of dried sugar beet pulp for binary biosorption of Gemazol Turquoise Blue-G reactive dye and copper (II) ions: equilibrium modeling. *Chemical Engineering Journal*, *127*(1-3), 177-188.

Alabi-Abass, O. M., Ibikunle, A. A., Lawal, S. O., Badejo, O. A., Awokoya, N. K., and Iriowen, M. E. (2016). Studies on the isolation, structural and functional properties of acetylated cellulose from the sandbox tree (Hura crepitans). *Int. J. Adv. Res.,* 4 (7), 865, 873.

Aljeboree, A. M., Alshirifi, A. N., and Alkaim, A. F. (2017). Kinetics and equilibrium study for the adsorption of textile dyes on coconut shell activated carbon. *Arabian journal of chemistry*, *10*, S3381-S3393.

Alemdar, A., and Sain, M. (2008b). Isolation and characterization of nanofibers from agricultural residues – Wheat straw and soy hulls. Bioresources Technology, 9,1664–1671.

Alshekhli, A. F., Hasan, H. A., Muhamad, M. H., and Abdullah, S. R. S. (2020). Development of adsorbent from phytoremediation plant waste for methylene blue removal. *Journal of Ecological Engineering*, *21*(8).

Alqaragully, M. B. (2014). Removal of textile dyes (maxilon blue, and methyl orange) by date stones activated carbon. *International Journal of Advanced Research in Chemical Science*, *1*(1), 48-59.

Arami, M., Limaee, N. Y., Mahmoodi, N. M., and Tabrizi, N. S. (2005a). Removal of dyes from colored textile wastewater by orange peel adsorbent: equilibrium and kinetic studies. *Journal of Colloid and interface Science*, *288*(2), 371-376.

Ayawei, N., Ebelegi, A. N., and Wankasi, D. (2017). Modelling and interpretation of adsorption isotherms. *Journal of Chemistry*, 2017: 1-11, (2017).

Azouaou, N., Sadaoui, Z., Djaafri, A. and Mokaddem, H., 2010. Adsorption of cadmium from aqueous solution onto untreated coffee grounds: Equilibrium, kinetics and thermodynamics. Journal of hazardous materials, 184(1-3), pp.126- 134.

Babarinde, A., Babalola, J. O., Adegoke, J., Osundeko, A. O., Olasehinde, S., Omodehin, A., and Nurhe, E. (2013). Biosorption of Ni (II), Cr (III), and Co (II) from solutions using Acalypha hispida leaf: kinetics, equilibrium, and thermodynamics. *Journal of Chemistry*, *2013*.

Bazrafshan, E., Mohammadi, L., Ansari-Moghaddam, A., and Mahvi, A. H. (2015). Heavy metals removal from aqueous environments by electrocoagulation process–a systematic review. *Journal of environmental health science and engineering*, *13*, 1-16.

Campos, N. F., Barbosa, C. M., Rodríguez-Díaz, J. M., and Duarte, M. M. (2018). Removal of naphthenic acids using activated charcoal: Kinetic and equilibrium studies. *Adsorption Science and Technology*, *36*(7-8), 1405-1421.

Chen, Y., Wang, F., Duan, L., Yang, H., and Gao, J. (2016). Tetracycline

adsorption onto rice husk ash, an agricultural waste: Its kinetic and thermodynamic studies. *Journal of Molecular Liquids*, *222*, 487-494.

Crini, G. (2006). Non-conventional low-cost adsorbents for dye removal: a review. *Bioresource technology*, *97*(9), 1061-1085.

Dada, A. O., Olalekan, A. P., Olatunya, A. M., and Dada, O. J. I. J. C. (2012). Langmuir, Freundlich, Temkin and Dubinin–Radushkevich isotherms studies of equilibrium sorption of Zn2+ unto phosphoric acid modified rice husk. *IOSR Journal of applied chemistry*, *3*(1), 38-45.

Değermenci, G. D., Değermenci, N., Ayvaoğlu, V., Durmaz, E., Çakır, D., and Akan, E. (2019). Adsorption of reactive dyes on lignocellulosic waste; characterization, equilibrium, kinetic and thermodynamic studies. *Journal of Cleaner Production*, *225*, 1220-1229.

de Lima, R. S., Tonholo, J., Rangabhashiyam, S., Fernandes, D. P., Georgin, J., de Paiva e Silva Zanta, C. L., and Meili, L. (2023). Enhancing Methylene Blue Dye Removal using pyrolyzed Mytella falcata Shells: Characterization, Kinetics, Isotherm, and Regeneration through Photolysis and Peroxidation. *Environmental Management*, 1-18.

El-Sikaily, A., El Nemr, A. and Khaled, A., 2011. Copper sorption onto dried red alga Pterocladia capillacea and its activated carbon. Chemical engineering journal, 168(2), pp.707-714

Enenebeaku, C. K., Okorocha, N. J., Enenebeaku, U. E., and Onyeachu, B. I. (2017). Adsorption of methylene blue dye onto bush cane bark powder. *International Letters of Chemistry, Physics and Astronomy*, *76*, 13.

Fernandes, E. P., Silva, T. S., Carvalho, C. M., Selvasembian, R., Chaukura, N., Oliveira, L. M., and Meili, L. (2021). Efficient adsorption of dyes by γ-alumina synthesized from aluminum wastes: Kinetics, isotherms, thermodynamics and toxicity assessment. *Journal of Environmental Chemical Engineering*, *9*(5), 106198.

Fernández-Ramos, M. D., Ogunneye, A. L., Babarinde, N. A. A., Erenas, M. M., and Capitán-Vallvey, L. F. (2020). Bioactive microfluidic paper device for pesticide determination in waters. *Talanta*, 218, 121108.

Fowomola, M. A. and Akindahunsi, A. A. (2007). Nutrients and Antinutrients of Hura crepitan seed. Journal of Medicinal Food, 10(1):159-164.

Gautam, R. K., Mudhoo, A., and Chattopadhyaya, M. C. (2013). Kinetic, equilibrium, thermodynamic studies and spectroscopic analysis of Alizarin Red S removal by mustard husk. *Journal of Environmental Chemical Engineering*, *1*(4), 1283-1291.

Georgin, J., Franco, D. S., Grassi, P., Tonato, D., Piccilli, D. G., Meili, L., and Dotto, G. L. (2019). Potential of Cedrella fissilis bark as an adsorbent for the removal of red 97 dye from aqueous effluents. *Environmental Science and Pollution Research*, *26*, 19207-19219.

Gierlinger, N., and Schwanninger, M. (2006). Chemical imaging of poplar wood cell walls by confocal Raman microscopy. *Plant physiology*, *140*(4), 1246-1254.

Ghosh K, Bar N, Biswas AB, Das SK. 2019. Removal of Methylene Blue (aq) using untreated and acid-treated

eucalyptus leaves and GAANN. Can J Chem Eng. 97(11):2883. doi:10.1002/cjce.23503.

Gulluce, E., Karadayi, M., Gulluce, M., Karadayi, G., Yildirim, V., Egamberdieva, D., and Alaylar, B. (2020). Bioremoval of methylene blue from aqueous solutions by Syringa vulgaris L. hull biomass. *Environmental Sustainability*, *3*, 303-312.

Hernandes, P. T., Oliveira, M. L., Georgin, J., Franco, D. S., Allasia, D., and Dotto, G. L. (2019). Adsorptive decontamination of wastewater containing methylene blue dye using golden trumpet tree bark (Handroanthus albus). *Environmental Science and Pollution Research*, *26*, 31924-31933.

Ho, Y. S., and McKay, G. (1999). Pseudo-second order model for sorption processes. *Process biochemistry*, *34*(5), 451-465.

Ibikunle, A. A., A. L. Ogunneye, N. O. Sanyaolu, K. A. Olutayo, S. A. Ogundare, A. O. Ogunmoye, O. C. Atewolara-Odule, S. T. Yussuf, and K. H. Moberuagba. "Application of modified cellulose for Pb^{2+} and Cu^{2+} removal from aqueous solutions: Kinetic and isotherms studies." *Scientia Africana* 22, no. 1 (2023): 115-132.

Iqbal, J., and Hussain, M. M. (2009). Intestinal lipid absorption. *American Journal of Physiology-Endocrinology and Metabolism*, *296*(6), E1183-E1194.

James, A.D. (2013) Phytochemical and Ethnabotical Analysis of Plants. Green Pharmarcy, Published Online www.arsgov/duke

Jawad AH, Rashid RA, Ishak MAM, Ismail K. 2018. Adsorptive removal of methylene blue by chemically treated cellulosic waste banana (Musasapientum) peels. J Taibah Univ Sci. 12(6):809–819. doi:10.1080/16583655.2018.1519893.

Jawad, A. H., and Abdulhameed, A. S. (2020). Mesoporous Iraqi red kaolin clay as an efficient adsorbent for methylene blue dye: adsorption kinetic, isotherm and mechanism study. *Surfaces and Interfaces*, *18*, 100422.

Jegede, M. M., Durowoju, O. S., and Edokpayi, J. N. (2021). Sequestration of hazardous dyes from aqueous solution using raw and modified agricultural waste. *Adsorption Science and Technology*, *2021*, 1-21.

Kalipci, E., Sahinkaya, S., Dortkol, M., and Aras, S. (2016). Decolorization of basic textile dyes using a novel adsorbent modification method: Ultrasonic-acid modification. *International Journal of Environmental Research*, *10*(1), 31-40.

Kebede, T. G., Mengistie, A. A., Dube, S., Nkambule, T. T., and Nindi, M. M. (2018). Study on adsorption of some common metal ions present in industrial effluents by Moringa stenopetala seed powder. *Journal of environmental chemical engineering*, *6*(1), 1378-1389.

Langmuir, I. (1918). The adsorption of gases on plane surfaces of glass, mica and platinum. *Journal of the American Chemical society*, *40*(9), 1361-1403.

Le, P. T., Bui, H. T., Le, D. N., Nguyen, T. H., Pham, L. A., Nguyen, H. N., ... and Le, T. P. Q. (2021). Preparation and characterization of biochar derived from agricultural by-products for dye removal. *Adsorption Science and Technology*, *2021*, 1-14.

Ma, J., Hou, L., Li, P., Zhang, S., and Zheng, X. (2022). Modified fruit pericarp as an effective biosorbent for removing

azo dye from aqueous solution: study of adsorption properties and mechanisms. *Environmental Engineering Research*, *27*(2).

Mahmoud MA, El-Halwany MM. 2014. Adsorption of cadmium to orange peels: isotherms, kinetics, and thermodynamics. *J Chromatogr Sep Tech.* 05(05):15. doi:10.4172/2157-7064.1000238.

Manzar, M. S., Khan, G., Saood Vanessa dos Santos Lins P, et al (2021) RSM-CCD optimization approach for the adsorptive removal of Eriochrome Black T from aqueous system using steel slag-based adsorbent: Characterization, Isotherm, Kinetic modeling and Thermodynamic analysis. J Mol Liq 116714. https://doi.org/10.1016/j.molliq.2021.116714

Mashkoor, F., and Nasar, A. (2020). Magnetized Tectona grandis sawdust as a novel adsorbent: preparation, characterization, and utilization for the removal of methylene blue from aqueous solution. *Cellulose*, *27*(5), 2613-2635.

McKew, B. A., Dumbrell, A. J., Taylor, J. D., McGenity, T. J., and Underwood, G. J. (2013). Differences between aerobic and anaerobic degradation of microphytobenthic biofilm-derived organic matter within intertidal sediments. *FEMS microbiology Ecology*, *84*(3), 495-509.

Meili, L., Lins, P. V. S., Costa, M. T., Almeida, R. L., Abud, A. K. S., Soletti, J. I., ... and Erto, A. (2019). Adsorption of methylene blue on agroindustrial wastes: experimental investigation and phenomenological modelling. *Progress in biophysics and molecular biology*, *141*, 60-71.

Meskel, A.G., Mussa, M., Meshesha, B.T., Habtu, N.G., Naik, S.V.C.S., V, B.P. (2023). Malachite Green and Methylene Blue Dye Removal Using Modified Bagasse Fly Ash: Adsorption Optimization Studies. Environmental Challenges, 14, 100829. DOI: 10.1016/j.envc.2023.100829.

Midha, V. A. R. S. H. A., and Dey, A. P. U. R. B. A. (2008). Biological treatment of tannery wastewater for sulfide removal. *International Journal of Chemical Sciences*, *6*(2), 472-486.

Mustapha, O. R., Osobamiro, T. M., Sanyaolu, N. O., and Alabi, O. M. (2023). Adsorption study of Methylene blue dye: an effluents from local textile industry using Pennisteum pupureum (elephant grass). *International Journal of Phytoremediation*, 1-11.

Nagy, B., Măicăneanu, A., Indolean, C., Mânzatu, C., Silaghi-Dumitrescu, L., and Majdik, C. (2014). Comparative study of Cd (II) biosorption on cultivated Agaricus bisporus and wild Lactarius piperatus based biocomposites. Linear and nonlinear equilibrium modelling and kinetics. *Journal of the Taiwan Institute of Chemical Engineers*, *45*(3), 921-929.

Ng, C., Losso, J. N., Marshall, W. E., and Rao, R. M. (2002). Freundlich adsorption isotherms of agricultural by-product-based powdered activated carbons in a geosmin–water system. *Bioresource technology*, *85*(2), 131-135.

Nithya, K., Sathish, A., Senthil Kumar, P., and Ramachandran, T. (2017). Functional group-assisted green synthesised superparamagnetic nanoparticles for the rapid removal of hexavalent chromium from aqueous solution. *IET Nanobiotechnology*, *11*(7), 852-860.

Nsi, E. W., Akpakpan, A. E., Ukpong, E. J., and Akpabio, U. D. (2016). Preparation and characterization of activated carbon from Hura Crepitans Linn seed shells. *The International Journal of Engineering and Science*, *5*(9), 38-41.

Ogundipe, K. D., and Babarinde, A. (2017). Comparative study on batch equilibrium biosorption of Cd (II), Pb (II) and Zn (II) using plantain (Musa paradisiaca) flower: kinetics, isotherm, and thermodynamics. *Chem. Int*, *3*(2), 135-149.

Ogunneye, A. L., Ibikunle, A. A., Sanyaolu, N. O., Yussuf, S. T., Gbadamosi, M. R., Badejo, O. A., and Lawal, O. S. (2020). Optimized carboxymethyl cellulose preparation from cocoa pod husks by surface response methodology. *Journal of Chemical Society of Nigeria*, *45*(1).

Oladipo, A. A., and Ifebajo, A. O. (2018). Highly efficient magnetic chicken bone biochar for removal of tetracycline and fluorescent dye from wastewater: two-stage adsorber analysis. *Journal of environmental management*, *209*, 9-16.

Oninla, V. O., Olatunde, A. M., Babalola, J. O., Adesanmi, O. J., Towolawi, G. S., and Awokoya, K. N., 2018. Qualitative assessments of the biomass from oil palm calyxes and its application in heavy metals removal from polluted water. *Journal of Environmental Chemical Engineering*, 6(4), pp.4044-4053.

Ooi, Jecksin, Lai Yee Lee, Billie Yan Zhang Hiew, Suchithra Thangalazhy-Gopakumar, Siew Shee Lim, and Suyin Gan. "Assessment of fish scales waste as a low cost and eco-friendly adsorbent for removal of an azo dye: Equilibrium, kinetic and thermodynamic studies." *Bioresource technology* 245 (2017): 656-664.

Parlayici, Ş. (2019). Alginate-coated perlite beads for the efficient removal of methylene blue, malachite green, and methyl violet from aqueous solutions: kinetic, thermodynamic, and equilibrium studies. *Journal of Analytical Science and Technology*, *10*(1), 1-15.

Patriota, S. N., Francisco, W., Araújo, D. F., and Mulholland, D. S. (2020). Adsorption of copper and methylene blue on an agrowaste of Mauritia flexuosa. *Journal of Environmental Engineering*, *146*(6), 04020039.

Paredes-Quevedo, L. C., González-Caicedo, C., Torres-Luna, J. A., and Carriazo, J. G. (2021). Removal of a textile azo-dye (Basic Red 46) in water by efficient adsorption on a natural clay. *Water, Air, and Soil Pollution*, *232*, 1-19.

Plazinski, W., Dziuba, J., and Rudzinski, W. (2013). Modeling of sorption kinetics: the pseudo-second order equation and the sorbate intraparticle diffusivity. *Adsorption*, *19*, 1055-1064.

Prado, A. G., Bolzon, L. B., Pedroso, C. P., Moura, A. O., and Costa, L. L. (2008). Nb2O5 as efficient and recyclable photocatalyst for indigo carmine degradation. *Applied Catalysis B: Environmental*, *82*(3-4), 219-224.

Sims, R. A., Harmer, S. L., and Quinton, J. S. (2019). The role of physisorption and chemisorption in the oscillatory adsorption of organosilanes on aluminium oxide. *Polymers*, *11*(3), 410.

Suganya, S. (2018). Influence of ultrasonic waves on preparation of active carbon from coffee waste for the reclamation of effluents containing Cr (VI)

ions. *Journal of Industrial and Engineering Chemistry*, *60*, 418-430.

Rangabhashiyam, S., dos Santos Lins, P. V., de Magalhães Oliveira, L. M., Sepulveda, P., Ighalo, J. O., Rajapaksha, A. U., and Meili, L. (2022). Sewage sludge-derived biochar for the adsorptive removal of wastewater pollutants: A critical review. *Environmental Pollution*, *293*, 118581.

Rudi N.N., Muhamad M.S., Chuan L. T., Alipal J., Omar S, Hamidon N, Abdul Hamid N. H., Sunar N. M., Ali R., Harun H. 2020. Evolution of adsorption process for manganese removal in water via agricultural waste adsorbents. *Heliyon.* 6(9): e05049. doi:10.1016/j.heliyon.

Simonin, J. P. (2016). On the comparison of pseudo-first order and pseudo-second order rate laws in the modeling of adsorption kinetics. *Chemical Engineering Journal*, *300*, 254-263.

Sasmal, S., Goud, V. V., and Mohanty, K. (2012). Characterization of biomasses available in the region of North-East India for production of biofuels. *Biomass and Bioenergy*, *45*, 212-220.

Ugwuoke, C. U., Monwuba, N., Onu, F. M., and Shimave, A. G. EN Okonkwo1 CC Opurum1 1. Department of Agricultural Education, University of Nigeria, Nsukka 2. Department of Agricultural Education, Federal University of Agriculture, Makurdi.

Viswanthan, S. P., Neelamury, S. P., Parakkuzhiyil, S., Njazhakunnathu, G. V., Sebastian, A., Padmakumar, B., and Ambatt, T. P. (2020). Removal efficiency of methylene blue from aqueous medium using biochar derived from Phragmites karka, a highly invasive wetland weed. *Biomass conversion and biorefinery*, 1-17.

Wang, S., Ang, H. M., and Tadé, M. O. (2008). Novel applications of red mud as coagulant, adsorbent and catalyst for environmentally benign processes. *Chemosphere*, *72*(11), 1621-1635.

Wang Q., Urbanization and global health: the role of air pollution, Iran J. Public Health 47 (2018) 1644–1652.

Yakar, A., Ünlü, A., Yeşilçayır, T., and Bıyık, İ. (2020). Kinetics and thermodynamics of textile dye removal by adsorption onto iron oxide nanoparticles. *Nanotechnology for Environmental Engineering*, *5*, 1-12.

Yudhanto, F., Yudha, V., and Syafri, E. (2023). Mechanical, Physical and Thermal Characterization of PVA (Polyvinyl Alcohol)/Chitosan Bioplastic Film. *International Journal of Heat and Technology*, *41*(3).

Zhang, X., Chen, S., Ramaswamy, S., Kim, Y. S., and Xu, F. (2017). Obtaining pure spectra of hemicellulose and cellulose from poplar cell wall Raman imaging data. *Cellulose*, *24*, 4671-4682.